

Deep Reinforcement Learning for Unmanned Aerial Vehicle-Assisted Vehicular Networks in Smart Cities

Ming Zhu*, Xiao-Yang Liu*, and Xiaodong Wang

Abstract—Unmanned aerial vehicles (UAVs) are envisioned to complement the 5G communication infrastructure in future smart cities. Hot spots easily appear in road intersections, where effective communication among vehicles is challenging. UAVs may serve as relays with the advantages of low price, easy deployment, line-of-sight links, and flexible mobility. In this paper, we study a UAV-assisted vehicular network where the UAV jointly adjusts its transmission power and bandwidth allocation under 3D flight to maximize the total throughput. First, we formulate a Markov Decision Process (MDP) problem by modeling the mobility of the UAV/vehicles and the state transitions. Secondly, we solve the target problem using a deep reinforcement learning method, namely, the deep deterministic policy gradient, and propose three solutions with different control objectives. Then we extend the proposed solutions considering of the energy consumption of 3D flight. Thirdly, in a simplified model with small state space and action space, we verify the optimality of proposed algorithms. Comparing with two baseline schemes, we demonstrate the effectiveness of proposed algorithms in a realistic model.

Index Terms—Unmanned aerial vehicle, vehicular networks, smart cities, Markov decision process, deep reinforcement learning, power control, bandwidth control.

I. INTRODUCTION

Intelligent transportation system [1] [2] [3] [4] [5] [6] is a key component of smart cities, which employs real-time data transmission for traffic monitoring, path planning, entertainment and advertisement [7]. High speed vehicular networks [8] emerge as a key component of intelligent transportation systems that provide cooperative communications to improve data transmission performance.

With the increasing number of vehicles, the current communication infrastructure may not satisfy data transmission requirements, especially when hot spots (e.g., road intersections) appear during rush hours. Unmanned aerial vehicles (UAVs) or drones [9] can complement the 4G/5G communication infrastructure, including vehicle-to-vehicle (V2V) communications, and vehicle-to-infrastructure (V2I) communications. Qualcomm has received a certification of authorization allowing for UAV testing below 400 feet [10]; Huawei will cooperate with China Mobile to build the first cellular test network for regional logistics UAVs [11].

*Contribute equally.

This work was supported by Leading Talents Program of Guangdong Province under grant 00201510, and the Shenzhen Peacock program under grant No. KQTD2015071715073798.

M. Zhu is with the Shenzhen Institutes of Advanced Technology, Chinese Academy of Sciences, Shenzhen 518055, China. E-mail: zhumingpassional@gmail.com.

X.-Y. Liu and X. Wang are with the Department of Electrical Engineering, Columbia University, New York, NY 10027, USA E-mail: {xiaoyang, wangx}@ee.columbia.edu.

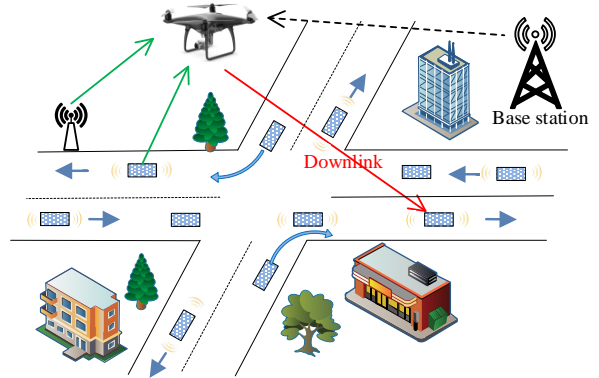


Fig. 1. The scenario of a UAV-assisted vehicular network.

A UAV-assisted vehicular network in Fig. 1 has several advantages. First, the path loss will be much lower since the UAV can move nearer to vehicles compared with stationary base stations. Secondly, the UAV is flexible in adjusting the transmission control [12] considering the mobility of vehicles. Thirdly, the quality of UAV-to-vehicle links is generally better than that of terrestrial links [13], since they are mostly line-of-sight (LoS).

Maximizing the total throughput of UAV-to-vehicle links has several challenges. First, the communication channels vary with the UAV's three-dimensional (3D) positions. Secondly, the joint adjustment of the UAV's 3D flight and transmission control (e.g., power and bandwidth control) cannot be solved directly using conventional optimization methods, especially when the environment is unknown. Thirdly, the channel conditions are hard to acquire, e.g., the path loss from the UAV to vehicles is closely related to the height/density of buildings and street width.

In this paper, we propose deep reinforcement learning based algorithms to maximize the total throughput of UAV-to-vehicle communications, which jointly adjusts the UAV's 3D flight and transmission control learned by interacting with the environment. The main contributions of this paper can be summarized as follows: 1) We formulate the problem as a Markov decision process (MDP) problem to maximize the total throughput with the constraints of total transmission power and total bandwidth; 2) We apply a deep reinforcement learning method, the deep deterministic policy gradient (DDPG), to solve the problem. DDPG is suitable to solve MDP problems with continuous states and actions. We propose three solutions with different control objectives to jointly adjust the UAV's 3D

flight and transmission control. Then we extend the proposed solutions considering of the energy consumption of 3D flight; 3) We verify the optimality of proposed solutions using a simplified model with small state space and action space. Finally, we provide extensive simulation results to demonstrate the effectiveness of the proposed solutions compared with two baseline schemes, namely, Cycle and Greedy.

The remainder of the paper is organized as follows. Section II discusses related works. Section III presents system models and problem formulation. Solutions are proposed in Section IV. Section V presents the performance evaluation. Section VI concludes this paper.

II. RELATED WORKS

The dynamic control for the UAV-assisted vehicular networks includes flight control and transmission control. Flight control mainly includes the planning of flight path, time, and direction. Yang *et al.* [14] proposed a joint genetic algorithm and ant colony optimization method to obtain the best UAV flight paths to collect sensory data in wireless sensor networks. To further minimize the UAVs' travel duration under certain constraints (e.g., energy limitations, fairness, and collision), Garraffa *et al.* [15] proposed a two-dimensional (2D) path planning method based on a column generation approach. Liu *et al.* [16] proposed a deep reinforcement learning approach to control a group of UAVs by optimizing the flying directions and distances to achieve the best communication coverage in the long run with limited energy consumption.

The transmission control of UAVs mainly concerns resource allocations, e.g., access selection, transmission power and bandwidth allocation. Wang *et al.* [17] presented a power allocation strategy for UAVs considering communications, caching, and energy transfer. In a UAV-assisted communication network, Yan *et al.* [18] studied a UAV access selection and base station bandwidth allocation problem, where the interaction among UAVs and base stations was modeled as a Stackelberg game, and the uniqueness of a Nash equilibrium was obtained.

Joint control of both UAVs' flight and transmission has also be considered. Wu *et al.* [19] maximized the minimum achievable rates from a UAV to ground users by jointly optimizing the UAV's 2D trajectory and power allocation. Zeng *et al.* [20] proposed a convex optimization method to optimize the UAV's 2D trajectory to minimize its mission completion time while ensuring each ground terminal recovers the file with high probability when the UAV disseminates a common file to them. Zhang *et al.* [21] minimized the UAV mission completion time by optimizing its 2D trajectory with a constraint on the connectivity quality from base stations to the UAV. However, most existing research works neglected adjusting UAVs' height to obtain better quality of links by avoiding various obstructions or non-line-of-sight (NLoS) links.

[22] optimized the UAV's 3D flight and transmission control together; however, the 3D position optimization was converted to a 2D position optimization by the LoS link requirement. The existing deep reinforcement learning based method only handle UAVs' 2D flight and simple transmission

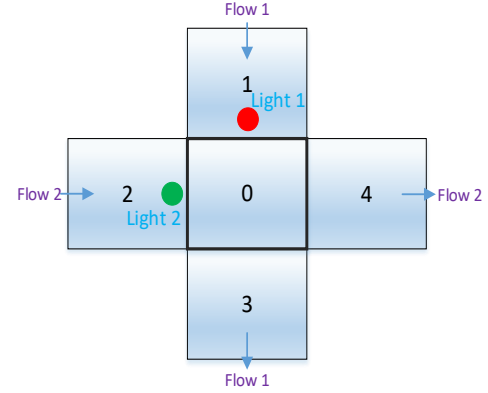


Fig. 2. A one-way-two-flow road intersection.

TABLE I
VARIABLES IN COMMUNICATION MODEL

h^i	channel power gain from UAV to a vehicle in block i .
ψ^i	SINR from the UAV to a vehicle in block i .
d_i, D_i	horizontal distance and Euclidean distance between the UAV and a vehicle in block i .
P, B	total transmission power and total bandwidth.
ρ^i, b^i	transmission power and bandwidth allocated for the vehicle in block i .

control decisions. For example, Challita *et al.* [23] proposed a deep reinforcement learning based method for a cellular UAV network by optimizing the 2D path and cell association to achieve a tradeoff between maximizing energy efficiency and minimizing both wireless latency and the interference on the path. A similar scheme is applied to provide intelligent traffic light control [24].

In addition, most existing works assumed that the ground terminals are stationary; whereas in reality, some ground terminals move with certain patterns, e.g., vehicles move under the control of traffic lights. This work studies a UAV-assisted vehicular network where the UAV's 3D flight and transmission control can be jointly adjusted, considering the mobility of vehicles in a road intersection.

III. SYSTEM MODELS AND PROBLEM FORMULATION

In this section, we first describe the traffic model and communication model, and then formulate the target problem as a Markov decision process. The variables in the communication model are listed in Table I for easy reference.

A. Traffic Model

We start with a one-way-two-flow road intersection, as shown in Fig. 2, while a much more complicated scenario in Fig. 7 will be evaluated in Section V. Five blocks are numbered as 0, 1, 2, 3, and 4, where block 0 is the intersection. We assume that each block contains at most one vehicle, indicated by binary variables $n^0, \dots, n^4 \in \{0, 1\}$. There are two traffic flows in Fig. 2,

- “Flow 1”: 1 → 0 → 3;
- “Flow 2”: 2 → 0 → 4.

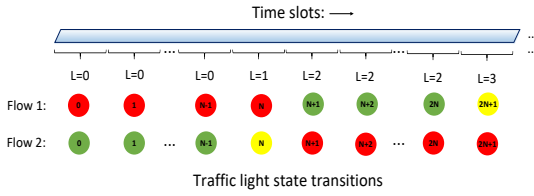


Fig. 3. Traffic light states along time.

The traffic light L has four configurations:

- $L=0$: red light for flow 1 and green light for flow 2;
- $L=1$: red light for flow 1 and yellow light for flow 2;
- $L=2$: green light for flow 1 and red light for flow 2;
- $L=3$: yellow light for flow 1 and red light for flow 2.

Time is partitioned into slots with equal duration. The duration of a green or red light occupies N time slots, and the duration of a yellow light occupies 1 time slot, which are shown in Fig. 3. We assume that each vehicle moves one block in a time slot if the traffic light is green.

B. Communication Model

We focus on the downlink communications (UAV-to-vehicle), since they are directly controlled by the UAV. There are two types of UAV-to-vehicle links, line-of-sight (LoS) and non-line-of-sight (NLoS). Let x and z denote the block (horizontal position) and height of the UAV respectively, where $x \in \{0, 1, 2, 3, 4\}$ corresponds to these five blocks in Fig. 2, and z is discretized to multiple values. Next, we describe the communication model, including the channel power gain, the signal to interference and noise ratio (SINR), and the total throughput.

Firstly, the channel power gain between the UAV and a vehicle in block i is h^i with a channel state $H^i \in \{\text{NLoS}, \text{LoS}\}$. h^i is formulated as [12] [25]

$$h^i = \begin{cases} D_i^{-\beta_1}, & \text{if } H^i = \text{LoS}, \\ \beta_2 D_i^{-\beta_1}, & \text{if } H^i = \text{NLoS}, \end{cases} \quad (1)$$

where D_i is the Euclidean distance between the UAV and the vehicle in block i , β_1 is the path loss exponent, and β_2 is an additional attenuation factor caused by NLoS connections.

The probabilities of LoS and NLoS links between the UAV and a vehicle in block i are [26]

$$p(H^i = \text{LoS}) = \frac{1}{1 + \alpha_1 \exp(-\alpha_2 (\frac{180}{\pi} \arctan \frac{z}{d_i} - \alpha_1))}, \quad (2)$$

$$p(H^i = \text{NLoS}) = 1 - p(H^i = \text{LoS}), \quad i \in \{0, 1, 2, 3, 4\}, \quad (3)$$

where α_1 and α_2 are system parameters depending on the environment, and d_i is the horizontal distance. The angle $\frac{180}{\pi} \arctan \frac{z}{d_i}$ is measured in “degrees” with the range $0^\circ \sim 90^\circ$. Both d_i and z are discrete variables, therefore, D_i is also a discrete variable.

Secondly, the SINR ψ_t^i in time slot t from the UAV to a vehicle in block i is characterized as [27]

$$\psi_t^i = \frac{\rho_t^i h_t^i}{b_t^i \sigma^2}, \quad i \in \{0, 1, 2, 3, 4\}, \quad (4)$$

where ρ_t^i and b_t^i are the allocated transmission power and bandwidth for the vehicle in block i in time slot t , respectively, and σ^2 is the additive white Gaussian noise (AWGN) power spectrum density, and h^i is formulated by (1). We assume that the UAV uses orthogonal frequency division multiple access (OFDMA) systems [28]; therefore, there is no interference among these channels.

Thirdly, the total throughput (reward) of UAV-to-vehicle links is formulated as [29]

$$\sum_{i \in \{0, 1, 2, 3, 4\}} b_t^i \log(1 + \psi_t^i) = \sum_{i \in \{0, 1, 2, 3, 4\}} b_t^i \log\left(1 + \frac{\rho_t^i h_t^i}{b_t^i \sigma^2}\right). \quad (5)$$

C. MDP Formulation

The UAV aims to maximize the total throughput with the constraints of total transmission power and total bandwidth:

$$\sum_{i \in \{0, 1, 2, 3, 4\}} \rho_t^i \leq P, \quad \sum_{i \in \{0, 1, 2, 3, 4\}} b_t^i \leq B,$$

where P is the total transmission power, and B is the total bandwidth, and $\rho_t^i \in [0, P]$, $b_t^i \in [0, B]$. We assume that there are totally κ channels. Therefore, $\frac{\rho_t^i \kappa}{B}$ must be an integer.

The target UAV-assisted communication problem is a Markov decision process (MDP) problem. On the one hand, from (1) we know that the channel power gain of UAV-to-vehicle links follows a stochastic process. On the other hand, the arrival of vehicles follows a stochastic process under the control of the traffic light.

Under the MDP framework, the state space \mathcal{S} , action space \mathcal{A} , reward r , policy π , and state transition probability $p(s_{t+1}|s_t, a_t)$ of our problem are defined as follows.

- State $\mathcal{S} = (L, x, z, n, H)$, where L is the traffic light state, (x, z) is the UAV’s 3D position with $x \in \{0, 1, 2, 3, 4\}$ being the block and z being the height, $n = (n^0, \dots, n^4)$ is the number of vehicles in those five blocks, and $H = (H^0, \dots, H^4)$ is the channel state from the UAV to each block $i \in \{0, 1, 2, 3, 4\}$ with $H^i \in \{\text{NLoS}, \text{LoS}\}$. Let $z \in [z_{\min}, z_{\max}]$, where z_{\min} and z_{\max} are the UAV’s minimum and maximum height, respectively. The block x is the location projected from UAV’s 3D position to the road networks.
- Action $\mathcal{A} = (\mathbf{f}, \rho, b)$ denotes the action set. \mathbf{f} is the UAV’s 3D flight, which includes horizontal and vertical flight. $\rho = (\rho_t^0, \dots, \rho_t^4)$ and $b = (b_t^0, \dots, b_t^4)$ are the transmission power and bandwidth allocation policies for those five blocks, respectively. At the end of time slot t , the UAV moves to a new 3D position according to action \mathbf{f} , and over time slot t , the transmission power and bandwidth are ρ and b , respectively.
- Reward $r(s_t, a_t) = \sum_{i \in \{0, 1, 2, 3, 4\}} b_t^i \log\left(1 + \frac{\rho_t^i h_t^i}{b_t^i \sigma^2}\right)$ is the total throughput (according to (4) and (5)) after a transition from state s_t to s_{t+1} taking action a_t . Note that the total throughput over the t -th time slot is measured at the state $s_t = (L_t, x_t, z_t, n_t, H_t)$.
- Policy π is the strategy for the UAV, which maps states to a probability distribution over the actions $\pi : \mathcal{S} \rightarrow \mathcal{P}(\mathcal{A})$, where $\mathcal{P}(\cdot)$ denotes probability distribution. In time slot t ,

the UAV's state is $s_t = (L_t, x_t, z_t, n_t, H_t)$, and its policy π_t outputs the probability distribution over the action a_t . We see that the policy indicates the action preference of the UAV.

- State transition probability $p(s_{t+1}|s_t, a_t)$ is the probability of the UAV entering the new state s_{t+1} , after taking the action a_t at the current state s_t . At the current state $s_t = (L_t, x_t, z_t, n_t, H_t)$, after taking the flight and transmission control $a_t = (\mathbf{f}, \rho, b)$, the UAV moves to the new 3D position (x_{t+1}, z_{t+1}) , and the channel state changes to H_{t+1} , with the traffic light changes to L_{t+1} and the number of vehicles in each block changes to n_{t+1} .

The state transitions of the traffic light along time are shown in Fig. 3. The state transition of the channel state for UAV-to-vehicle links is a stochastic process, which is reflected by (2) and (3).

Next, we discuss the MDP in two aspects: the state transitions of the number of vehicles in each block, and the UAV's 3D position. Note that the transmission power and bandwidth allocations do not affect the traffic light, the channel state, the number of vehicles, and the UAV's 3D position.

Firstly, we discuss the state transitions of the number of vehicles in each block. It is a stochastic process. The UAV's states and actions do not affect the number of vehicles of all blocks, thus, they are not shown. Let λ_1 and λ_2 be the probability of the arrivals of new vehicles in flow 1 and 2, and $\{n_t^i\}_{i \in \{0,1,2,3,4\}}$ be the number of vehicles in each block in time slot t .

The state transitions for the number of vehicles in block 0, 3, and 4 are

$$n_{t+1}^0 = \begin{cases} n_t^2, & \text{if } L_t = 0, \\ n_t^1, & \text{if } L_t = 2, \\ 0, & \text{otherwise,} \end{cases} \quad (6)$$

$$n_{t+1}^3 = \begin{cases} n_t^0, & \text{if } L_t = 2, 3, \\ 0, & \text{otherwise,} \end{cases} \quad (7)$$

$$n_{t+1}^4 = \begin{cases} n_t^0, & \text{if } L_t = 0, 1, \\ 0, & \text{otherwise.} \end{cases} \quad (8)$$

The transition probability is 1 in (6), (7) and (8) since the transitions are deterministic. While state transition probabilities for the number of vehicles in block 1 and 2 are stochastic, moreover, both of them are affected by their current number of vehicles and the traffic light. We take block 1 as an example when the traffic light state is $L_t = 2$

$$p(n_{t+1}^1 = 1|L_t = 2) = \lambda_1, \quad (9)$$

$$p(n_{t+1}^1 = 0|L_t = 2) = 1 - \lambda_1. \quad (10)$$

When $(n_t^1 = 0, L_t \neq 2)$ and $(n_t^1 = 1, L_t \neq 2)$, the state transition probability will be obtained in a similar way.

Secondly, we discuss the state transition of the UAV's 3D position. It includes block transitions and height transitions. We assume that the UAV's block and height in time slot t are x_t and z_t , respectively. The UAV's new height is its current

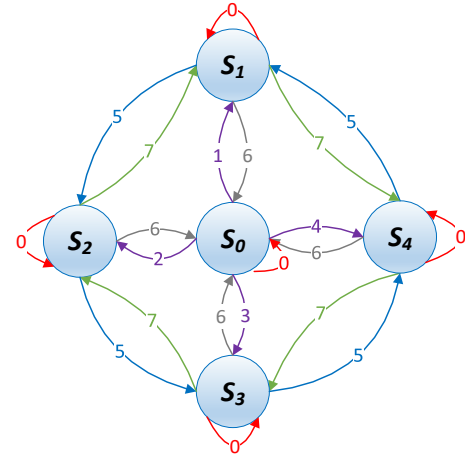


Fig. 4. The state transition diagram when the UAV's height is fixed.

height plus its vertical flight. If the UAV's height is fixed, the corresponding position state transition diagram is shown in Fig. 4, where $\{S_i\}_{i \in \{0,1,2,3,4\}}$ denotes the block of the UAV: 0 denotes staying in the current block; $\{1, 2, 3, 4\}$ denotes a flight from block 0 to the other blocks (1, 2, 3, and 4); 5 denotes an anticlockwise flight; 6 denotes a flight to block 0 from the other blocks; 7 denotes a clockwise flight.

In our problem, $\alpha_1, \alpha_2, \beta_1, \beta_2, \lambda_1$, and λ_2 are unknown. $\alpha_1, \alpha_2, \beta_1$, and β_2 are related to height/density of buildings, street width, and the weather, etc. λ_1 and λ_2 are related to traffic flows. This problem can not be solved directly using conventional MDP solutions. In the next section, we describe proposed solutions in detail.

IV. PROPOSED SOLUTIONS

In this section, we first present an overview of Q-learning and the deep deterministic policy gradient algorithm, and then propose solutions with different control objectives, and finally present the extension on energy consumption of 3D flight.

A. Q-learning

Q-learning [30] is a classic method of model-free RL [31]. RL can solve standard MDP problems. The return from a state is defined as the sum of discounted future reward $\sum_{i=t}^{T'} \gamma^{i-t} r(s_i, a_i)$, where T' is the total number of time slots, and $\gamma \in (0, 1)$ is a discount factor that diminishes the future reward and ensures that the sum of an infinite number of rewards is still finite. RL with the essence of exploration and exploitation aims to maximize the expected return from an initial distribution by interacting with the environment. Many RL approaches use the recursive relationship known as Bellman equation for action-value function [32]:

$$Q^\pi(s_t, a_t) = r(s_t, a_t) + \gamma \sum_{s_{t+1}} p(s_{t+1}|s_t, a_t) \max_{a_{t+1}} Q^\pi(s_{t+1}, a_{t+1}),$$

where $Q^\pi(s_t, a_t)$ value represents the expected return after taking action a_t in state s_t under policy π .

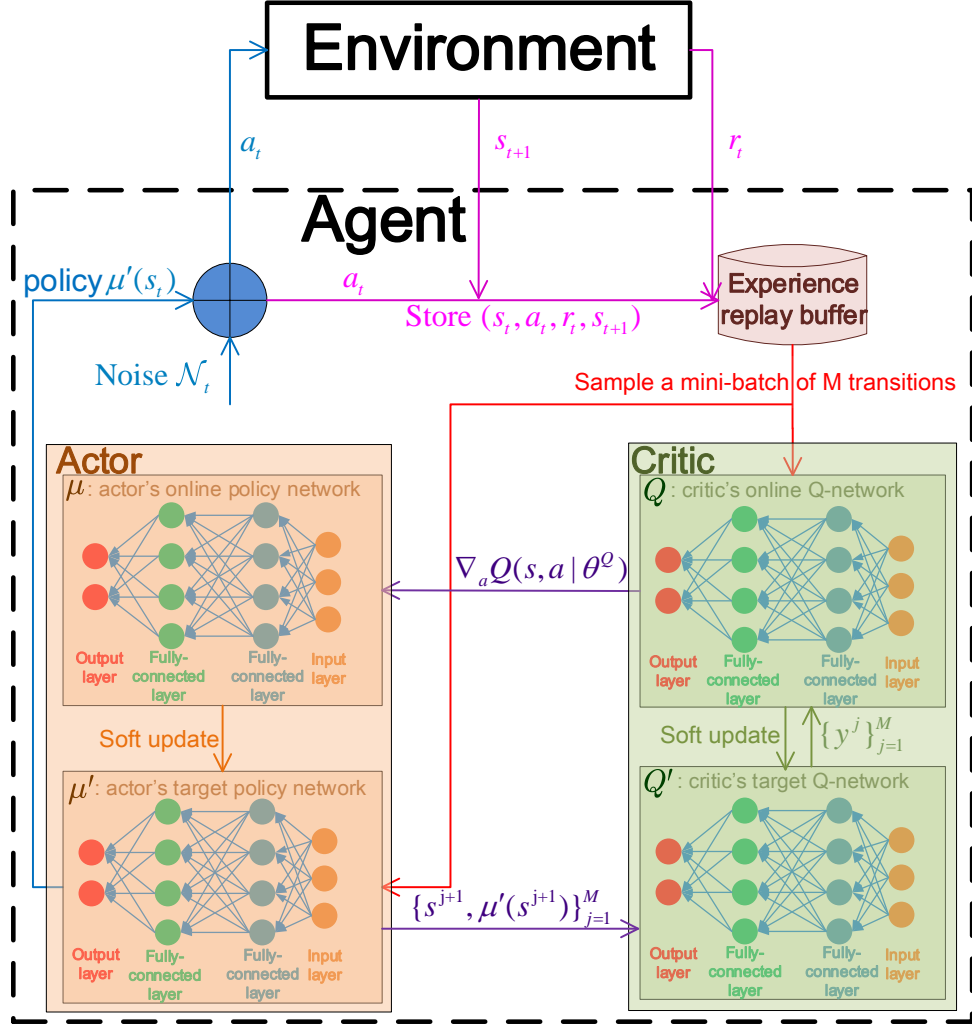


Fig. 5. Framework of the DDPG algorithm.

Q-learning [33] uses a greedy policy to get a new action $\arg \max_{a_t} Q(s_t, a_t)$. The update equation of $Q(s_t, a_t)$ is

$$Q(s_t, a_t) \leftarrow Q(s_t, a_t) + \alpha \left[r_{t+1} + \max_{a_{t+1}} Q(s_{t+1}, a_{t+1}) - Q(s_t, a_t) \right],$$

where α is a learning rate.

Classic RL algorithms such as Q-learning use value functions (state value function $V(s)$ or action value function $Q(s, a)$) to estimate the expected return. The function can be defined by a tabular mapping of discrete inputs to outputs. However, this is impossible for continuous or a large number of states/actions, since classic RL will converge with too much memory and computation resources. Function approximation is suitable for a large state/action space. A function approximation method is deep neural networks.

B. Deep Deterministic Policy Gradient

Deep deterministic policy gradient (DDPG) [34] in Fig. 5 is a type of deep RL, which uses deep neural networks to approximate both action policy and Q-value. It has exploited the powerful skills introduced in AlphaGo zero [35] and Atari

game playing [36]. DDPG is much more efficient and performs better in a high dimensional task than the stochastic policy gradient [24] [37]. DDPG's actor-critic approach can solve the MDP with continuous action space: the actor approximates the action policy, and the critic approximates the Q-value.

The actor has two neural networks: the online policy network μ (parameter: θ^μ) with state s as input and action $\mu(s)$ as output and the target policy network μ' (parameter: $\theta^{\mu'}$) with θ^μ as input and action $\mu'(s)$ as output. The online policy network μ is updated following the chain rule for the expected return J from the initial distribution with respect to the actor's parameters θ^μ :

$$\begin{aligned} \nabla_{\theta^\mu} J &= \mathbb{E}_{s_t \sim \eta^\beta} [\nabla_{\theta^\mu} Q(s, a | \theta^Q) |_{s=s_t, a=\mu(s_t | \theta^\mu)}] \\ &= \mathbb{E}_{s_t \sim \eta^\beta} [\nabla_a Q(s, a | \theta^Q) |_{s=s_t, a=\mu(s_t | \theta^\mu)} \nabla_{\theta^\mu} \mu(s | \theta^\mu) |_{s=s_t}], \end{aligned} \quad (11)$$

where η^β is the state visitation distribution on the policy β . The target policy network μ' is updated by slowly tracking the online policy network μ : $\theta^{\mu'} \leftarrow \tau \theta^\mu + (1 - \tau) \theta^{\mu'}$, where $\tau \ll 1$ is a low learning rate.

Algorithm 1: DDPG-based algorithms: PowerControl, BandControl, and JointControl

Input: the number of episodes K , the number of timesteps T in an episode, the mini-batch size M , the learning rate τ ;

- 1: Initialize all states, including the traffic light state L , the UAV's 3D position (x, z) , the number of vehicles n and the channel state H in all blocks, and then set the dimension of states;
- 2: Set the dimension of the UAV's actions DDPG controls in PowerControl, BandControl, or JointControl;
- 3: Randomly initialize critic's online Q-network parameters θ^Q and actor's online policy network parameters θ^μ , and initialize the critic's target Q-network parameters $\theta^{Q'} \leftarrow \theta^Q$ and actor's target policy network parameters $\theta^{\mu'} \leftarrow \theta^\mu$;
- 4: Initialize the UAV's experience replay buffer R_b ;
- 5: **for** episode $k = 1$ to K
- 6: Initialize a random process (a standard normal distribution) \mathcal{N} for the UAV's action exploration;
- 7: Observe the initial state s_1 ;
- 8: **for** $t = 1$ to T
- 9: Select the UAV's action $a_t = \mu'(s_t | \theta^{\mu'}) + \mathcal{N}_t$ according to the current policy and exploration noise \mathcal{N}_t ;
- 10: **if** PowerControl
- 11: Add the equal bandwidth allocation policy as part of the UAV's action;
- 12: **if** BandControl
- 13: Add the equal transmission power allocation policy as part of the UAV's action;
- 14: Execute the UAV's action, and receive reward r_t , and observe new state s_{t+1} from the environment;
- 15: Store transition (s_t, a_t, r_t, s_{t+1}) in the UAV's experience replay buffer R_b ;
- 16: Sample a random mini-batch of M transitions $\{(s^j, a^j, r^j, s^{j+1})\}_{j=1}^M$ from the UAV's experience replay buffer R_b ;
- 17: Set $y^j = r^j + \gamma Q'(s^{j+1}, \mu'(s^{j+1} | \theta^{\mu'}) | \theta^{Q'})$;
- 18: Update the critic's online Q-network (i.e., the evaluation of the UAV's actions) by minimizing the loss function:

$$\nabla_{\theta^Q} \text{Loss}(\theta^Q) = \nabla_{\theta^Q} \left[\frac{1}{M} \sum_{j=1}^M (y^j - Q(s^j, a^j | \theta^Q))^2 \right];$$
- 19: Update the actor's online policy network (i.e., the UAV's policy) using the policy gradient by the chain rule:

$$\nabla_{\theta^\mu} J \approx \frac{1}{M} \sum_{j=1}^M \nabla_a Q(s, a | \theta^Q) |_{s=s^j, a=\mu(s^j)} \nabla_{\theta^\mu} \mu(s | \theta^\mu) |_{s=s^j};$$
- 20: Soft update the critic's target Q-network Q' and actor's target policy network μ' to make the evaluation of the UAV's actions and the UAV's policy more stable: $\theta^{Q'} \leftarrow \tau \theta^Q + (1 - \tau) \theta^{Q'}$, $\theta^{\mu'} \leftarrow \tau \theta^\mu + (1 - \tau) \theta^{\mu'}$;

The critic also has two neural networks: the online Q-network Q (parameter: θ^Q) with a state-action pair (s, a) as input and Q-value $Q(s, a)$ as output and the target Q-network Q' (parameter: $\theta^{Q'}$) with θ^Q as input and Q-value $Q'(s, a)$ as output. It helps to evaluate the actions of the actor. The online Q-network (i.e., the evaluation of the UAV's actions) is updated by minimizing the loss function:

$$\nabla_{\theta^Q} \text{Loss}(\theta^Q) = \nabla_{\theta^Q} \left[\frac{1}{M} \sum_{j=1}^M (y^j - Q(s^j, a^j | \theta^Q))^2 \right], \quad (12)$$

where

$$y^j = r^j + \gamma Q'(s^{j+1}, \mu'(s^{j+1} | \theta^{\mu'}) | \theta^{Q'}). \quad (13)$$

The target Q-network Q' is updated by slowly tracking the online Q-network Q : $\theta^{Q'} \leftarrow \tau \theta^Q + (1 - \tau) \theta^{Q'}$.

DDPG uses three skills to guarantee the UAV's communication performance and stability: experience replay buffer, soft update, and exploration noise.

Experience replay buffer R_b stores transitions that will be used for model update. Note that there are correlations between the UAV's consecutive transitions, leading to extremely slow convergence. DDPG stores each transition (s_t, a_t, r_t, s_{t+1}) in R_b , and then uniformly samples a mini-batch of M transitions, and executes stochastic gradient decent [38] to update network weights for the critic network $Q(s, a)$. "Experience replay buffer" has two advantages: 1) enabling the stochastic gradient decent method; 2) and removing the correlations between consecutive transitions.

Soft update (parameter $\tau \ll 1$) is introduced for the target policy network μ' and the target Q-network Q' , which makes them more stable. They are updated according to μ and Q . This process makes the total throughput of the UAV-to-vehicle links more stable in the scenario of time-varying vehicle flows.

Exploration noise \mathcal{N}_t is added to the target policy to get a new action, i.e., $a_t = \mu'(s_t | \theta^{\mu'}) + \mathcal{N}_t$. It solves the tradeoff between exploration and exploitation, and the exploration is independently from the learning process. This ensures that the UAV has a certain probability of exploring other actions besides the one predicted by the current policy, and avoid that the UAV is trapped in a local optimum.

C. Deep Reinforcement Learning-based Solutions

We propose solutions using DDPG since it is able to learn continuous states/actions such as transmission power allocation. The UAV does not know the exact traffic and communication coefficients; however, through a series of trials or errors, the action value and policy can be approximated using deep neural networks in stead of tabular functions. Moreover, the proposed solutions converge with much less memory and computation resources compared with Q-learning. Therefore, we choose DDPG to solve our problem.

The usage of DDPG has two stages: training and test. Firstly, the UAV enters the training stage. We train the neural networks of the actor and critic in Algorithm 1, and stores the weights and biases of all neural networks when they converge.

Secondly, the UAV enters the test stage. We restore all neural networks, and then use the actor's target policy network μ' to output the policy according to the current state. Note that there is no noise added to μ' , since the UAV has got the optimal policy through DDPG. Finally, the UAV executes this policy.

The workflow of DDPG in the training stage is shown in Fig. 5. It mainly uses four components of DDPG: experience replay buffer, actor, critic, and exploration noise. The UAV receives the reward r_t and new state s_{t+1} from the environment after taking action a_t in state s_t , and then the state transition is stored in the experience replay buffer R_b . A mini-batch of M transitions are sampled from R_b for the actor's target policy network μ' and the critic's online Q-network Q . μ' outputs $\{s^{j+1}, \mu'(s^{j+1})\}_{j=1}^M$ to the critic's target Q-network Q' to calculate the target label $\{y^j\}_{j=1}^M$. Q calculates $\nabla_s Q(s, a | \theta^Q)$ for the actor's online policy network μ . Q' and μ' soft update themselves. μ' outputs its policy $\mu'(s_t)$. Then an exploration noise \mathcal{N}_t is added to the target policy μ' to get an action of the UAV.

Despite the UAV's 3D flight control, the UAV has two communication controls, power and bandwidth. We assume the UAV can either choose power or bandwidth control, and then we propose three algorithms:

- PowerControl: the UAV adjusts its 3D flight and the transmission power allocation using the actor network, and the bandwidth are equally allocated to each vehicle in each time slot.
- BandControl: the UAV adjusts its 3D flight and bandwidth allocation using the actor network, and the transmission power is equally allocated to each vehicle in each time slot.
- JointControl: the UAV adjusts its 3D flight, the transmission power and bandwidth allocation using the actor network.

The DDPG-based algorithms are given in **Algorithm 1**. We describe the algorithm into two parts: initializations, the main process of DDPG.

First, we describe the initializations in lines 1 ~ 4. In line 1, all states are initialized and then the dimension of states is initialized: the traffic light L is initialized as 0, the UAV's initial 3D position is the intersection block with a predefined height, the number of vehicles n in all blocks is 0, and the channel state H is set as LoS. Line 2 sets the dimension of the UAV's actions DDPG controls in PowerControl, BandControl, and JointControl, which is different among them. Line 3 initializes the parameters of the critic and actor. Line 4 initializes the experience replay buffer R_b .

Secondly, we present the main process of DDPG. Line 6 initializes a random process for action exploration. Line 7 receives an initial state s_1 . Line 9 selects an action according to the current policy and exploration noise. The dimension of actions DDPG controls in three solutions is different. Lines 10 ~ 11 add the equal bandwidth allocation policy in PowerControl. Lines 12 ~ 13 add the equal power allocation policy in BandControl. Line 14 executes the UAV's action, and then the reward and all states will be updated. Line 15 stores the UAV's experience into R_b . In line 16, a random

mini-batch will be sampled uniformly. Line 17 sets the target label y^j . Line 18 updates the critic's online Q-network, and line 19 updates the actor's online policy network. Lines 20 updates the critic's target Q-network, and the actor's target policy network.

There are several types of parameters needed to be properly tuned to achieve convergence in the training stage.

- Weight and bias initialization is important in DDPG. The aim of weight and bias initialization is to prevent layer activation outputs from exploding or vanishing during the course of a forward pass through a deep neural network. Recently years, pretraining is not so necessary to achieve convergence due to rectified linear activation units (ReLUs) [39]. ReLU or leaky ReLU exploding gradients can be solved with the He initialization [40], which is comparatively better than old techniques and is used in our problem.
- The configure of fully-connected layers in proposed solutions is based on the configure of the DDPG action space. A neural network consists of an input layer, fully-connected layers, and an output layer. The number of fully-connected layers in actor is set to 8, and the dimension of the output space is set to 10 of the dimension of actions DDPG controls.
- The setting of the exploration noise is related to the current policies. Generally, the output of a neural network is $[-1, 1]$, and the noise is assumed to follow a standard normal distribution, i.e., a mean of 0 and a standard deviation of 1. Moreover, to facilitate getting higher-quality training data and speed the convergence of neural networks, we assume that in each time slot the exploration noise declines with a very low rate.

D. Extension on Energy Consumption of 3D Flight

The UAV's energy is used in two parts, communication and 3D flight. The above proposed solutions of the last subsection do not consider the energy consumption of 3D flight, which may be much larger than that in communication. In this subsection, we discuss how to incorporate the energy consumption of 3D flight into the proposed deep reinforcement learning solutions. To encourage or discourage the UAV's 3D flight actions in different directions with different amount of energy consumption, we revise the reward function. The basic idea is inspired by [41].

The reward function is modified as follows

$$\bar{r}(s_t, a_t) = \frac{1}{e} \sum_{i \in \{0, 1, 2, 3, 4\}} b_t^i \log(1 + \frac{\rho_t^i h_t^i}{b_t^i \sigma^2}), \quad (14)$$

where e is the energy consumption of taking action a_t in a time slot. The Q-value is updated by the following rule

$$Q(s_t, a_t) \leftarrow Q(s_t, a_t) + \alpha \delta(t), \quad (15)$$

where α is a learning rate, and $\delta(t)$ is a prediction error as follows

$$\delta(t) = \bar{r}(s_t, a_t) - Q(s_t, a_t). \quad (16)$$

The modified Q-learning model is formulated as [41]

$$Q(s_t, a_t) \leftarrow Q(s_t, a_t) + \begin{cases} \alpha^+ \delta(t), & \text{if } \delta(t) \geq 0, \\ \alpha^- \delta(t), & \text{if } \delta(t) < 0. \end{cases} \quad (17)$$

The corresponding deep reinforcement learning model is

$$Q(s_t, a_t | \theta^Q) \leftarrow Q(s_t, a_t | \theta^Q) + \begin{cases} \alpha^+ \delta(t), & \text{if } \delta(t) \geq 0, \\ \alpha^- \delta(t), & \text{if } \delta(t) < 0, \end{cases} \quad (18)$$

where θ^Q is the model parameters. Then we optimize it by the loss function:

$$\nabla_{\theta^Q} \text{Loss}(\theta^Q) = \nabla_{\theta^Q} \left[\frac{1}{M} \sum_{j=1}^M (y^j - Q(s^j, a^j | \theta^Q))^2 \right], \quad (19)$$

where

$$y^j = \bar{r}^j. \quad (20)$$

If $\alpha^+ > \alpha^-$, the UAV is active and prefers to move. If $\alpha^+ < \alpha^-$, the UAV is inactive and prefers to stay. If $\alpha^+ = \alpha^-$, the UAV is neither active nor inactive. The probability of selecting an action is estimated by the typical softmax rule. The algorithms considering of energy consumption of 3D flight can be easily reflected from Algorithm 1 by the above modifications.

V. PERFORMANCE EVALUATION

For a one-way-two-flow road intersection in Fig. 2, we present the optimality verification of deep reinforcement learning algorithms. Then, we study a more realistic road intersection as shown in Fig. 7, and present our simulation results.

Our simulations are executed on a server with Linux OS, 200 GB memory, two Intel(R) Xeon(R) Gold 5118 CPUs@2.30 GHz, a Tesla V100-PCIE GPU and four RTX 2080 Ti GPUs.

The implementation of Algorithm 1 includes two parts: building the environment (including traffic and communication models) for our scenarios, and using the DDPG algorithm in TensorFlow [42].

A. Optimality Verification of Deep Reinforcement Learning

Theoretically, it is well-known that deep reinforcement learning algorithms (including DDPG algorithms) solve MDP problems and achieve the optimal results with much less memory and computation resources. We provide the optimality verification of DDPG-based algorithms in Algorithm 1 in a one-way-two-flow road intersection in Fig. 2. The reasons are as follows: (i) the MDP problem in such a simplified scenario is explicitly defined and the theoretically optimal policy can be obtained using the Python MDP Toolbox [43]; and (ii) this optimality verification process also serves a good code debugging process before we apply the DDPG algorithm in TensorFlow [42] to the more realistic road intersection scenario in Fig. 7.

The assumptions and settings of the simplified scenario in Fig. 2 are as follows. To keep the state space small for verification purpose, we assume the channel states of all communication links are LoS, and the UAV's height is fixed

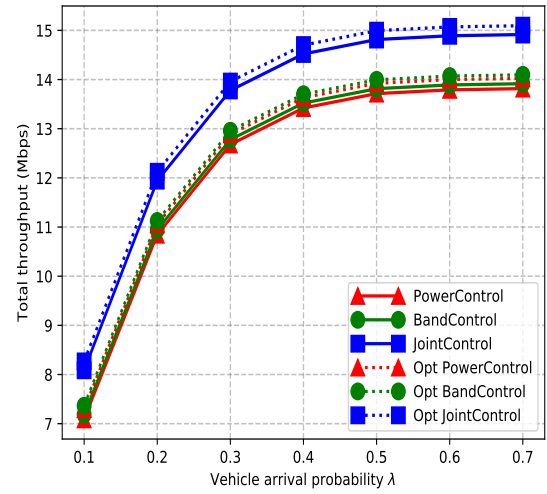


Fig. 6. Total throughput vs. vehicle arrival probability λ in optimality verification.

as 150 meters, so that the UAV can only adjust its horizontal flight control and transmission control. The traffic light state is assumed to have two values (red or green). The power and bandwidth allocation actions for each block i have three values, and the total number of channels κ is 256, and the vehicle arrival probabilities for block 1 and 2 are the same and are in the range $0.1 \sim 0.7$, and the discount factor γ is 0.9.

The result of DDPG-based algorithms matches that of the policy iteration algorithm using Python MDP Toolbox [43] (serving as the optimal policy). The total throughput obtained by the policy iteration algorithm and DDPG-based algorithms are shown as dashed lines and solid lines in Fig. 6. Therefore, DDPG-based algorithms achieve near optimal policies. We see that, the total throughput in JointControl is the largest, which is much higher than PowerControl and BandControl. This is in consistent with our believes that the JointControl of power and bandwidth allocation will be better than the control of either of both. The performance of PowerControl is almost the same as BandControl, since the power and bandwidth almost have the same effects on communication performance. The throughput increases with the increasing of vehicle arrival probability λ in all algorithms, and it saturates when $\lambda \geq 0.6$ due to traffic congestion.

B. More Realistic Traffic Model

We consider a more realistic road intersection model in Fig. 7. There are totally 33 blocks with four entrances (block 26, 28, 30, and 32), and four exits (block 25, 27, 29, and 31). Vehicles in block $i \in \{2, 4, 6, 8\}$ go straight, turn left, turn right with the probabilities g_i^s , g_i^l , and g_i^r , such that $g_i^s + g_i^l + g_i^r = 1$. We assume vehicles can turn right when the traffic light is green. We assume $\{n^j\}_{j \in \{26, 28, 30, 32\}}$ follows a binomial distribution with the same parameter λ . The blocks' distance is easily calculated as follows: $D(1, 2) = \hat{d}$, and

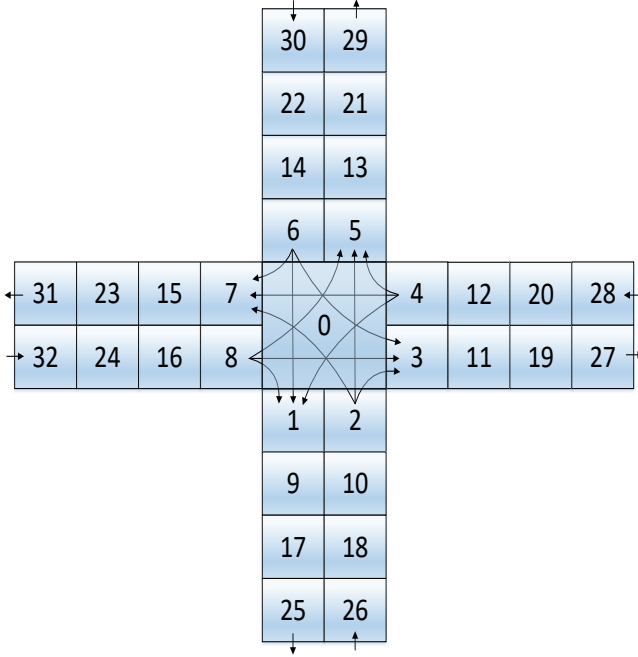


Fig. 7. Realistic road intersection model.

$D(1, 6) = 3\hat{d}$, where $D(i, j)$ is the Euclidean distance from block i to block j , and \hat{d} is the length of a block.

The UAV's horizontal flight actions are as follows. We assume that the UAV's block is $0 \sim 8$ since the number of vehicles in the intersection block 0 is generally the largest and the UAV will not move to the block far from the intersection block. Moreover, within a time slot we assume that the UAV can stay or only move to its adjacent blocks.

The parameter settings are summarized in Table II. In the simulations, there are three types of parameters: DDPG algorithm parameters, communication parameters, and UAV/vehicle parameters.

First, we describe the DDPG algorithm parameters. The number of episodes is 256, and the number of timesteps in an episode is 256, so the number of total time slots is 65,536. The experience replay buffer capacity is 10,000, and the learning rate of target networks τ is 0.001. The discount factor γ is $0.4 \sim 0.9$, and the mini-batch size M is 512.

Secondly, we describe communication parameters. α_1 and α_2 are set to 9.6 and 0.28, which are common values in urban areas [44]. β_1 is 3, and β_2 is 0.01, which are widely used in path loss modeling. The duration of a time slot is set to 6 seconds, and the number of occupied red or green traffic light N is 10, i.e., 60 seconds constitute a red/green duration, which is commonly seen in cities and can ensure that the vehicles in blocks can get the next block in a time slot. The white power spectral density σ^2 is set to -130 dBm/Hz. The total UAV transmission power P is set to $1 \sim 6$ W in consideration of the limited communication ability. The total bandwidth allocated for vehicles B is $0.5 \sim 1$ MHz.

Thirdly, we describe UAV/vehicle parameters. The maximum vertical distance that the UAV can move in a time slot is set to 5 meters considering of its speed. The minimum and

TABLE II
VALUES OF PARAMETERS IN SIMULATION SETTINGS

α_1	α_2	β_1	β_2	σ^2	\hat{d}
9.6	0.28	3	0.01	-130 dBm/Hz	3
P	B	N	γ	z_{\min}	z_{\max}
$1 \sim 6$	$0.5 \sim 1$ MHz	10	$0.4 \sim 0.9$	10	200
M	λ	g_i^s	g_i^l	g_i^r	κ
512	$0.1 \sim 0.7$	0.4	0.3	0.3	256
τ					
0.001					

maximum height of the UAV is 10 meters and 200 meters. The interval of the UAV height is 5 meters. λ is set to $0.1 \sim 0.7$. The length of a road block \hat{d} is set to 3 meters. The probability of a vehicle going straight, turning left, and turning right (g_i^s , g_i^l , and g_i^r) is set to 0.4, 0.3, and 0.3, respectively, and each of them is assumed to be the same in block 2, 4, 6, and 8. The total number of channels κ is 256.

C. Baseline Schemes

We compare with two baseline schemes. Generally, the equal transmission power and bandwidth allocation is common in communication systems for fairness. Therefore, they are used in baseline schemes.

The first baseline scheme is Cycle, i.e., the UAV cycles anticlockwise at a fixed height (e.g., 150 meters), and the UAV allocates the transmission power and bandwidth equally to each vehicle in each time slot. The UAV moves along the fixed trajectory periodically, without considering the vehicle flows.

The second baseline scheme is Greedy, i.e., at a fixed height (e.g., 150 meters), the UAV greedily moves to the block with the largest number of vehicles. If a nonadjacent block has the largest number of vehicles, the UAV has to move to block 0 and then move to that block. The UAV also allocates the transmission power and the bandwidth equally to each vehicle in each time slot. The UAV tries to serve the block with the largest number of vehicles by moving nearer to them.

D. Simulation Results

Next, we first show the convergence of loss functions, and then show total throughput vs. discount factor, total transmission power, total bandwidth and vehicle arrival probability, and finally present the UAV's flight time vs. energy percent for 3D flight.

The convergence of loss functions in training stage for PowerControl, BandControl, and JointControl indicates that the neural network is well-trained. It is shown in Fig. 8 when $P = 6$, $B = 1$ MHz, $\lambda = 0.5$ and $\gamma = 0.9$ during time slot 12,000 \sim 13,000. The first 12,000 time slots are not shown since during the 0 \sim 12,000, the experience replay buffer has not achieved its capacity, and from 10,000 \sim 12,000, the fluctuation is large just after the R_b is full. We see that, the loss functions in three algorithms converge after 12,000 time slots. The other metrics in the paper are measured in test stage by default.

Total throughput vs. discount factor γ is drawn in Fig. 9 when $P = 6$, $B = 1$ MHz, and $\lambda = 0.5$. We can see that,

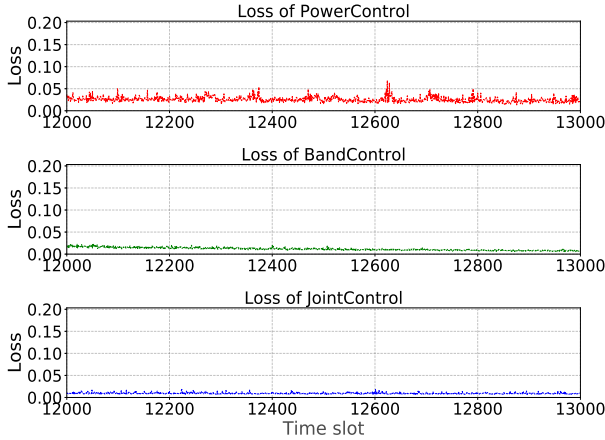
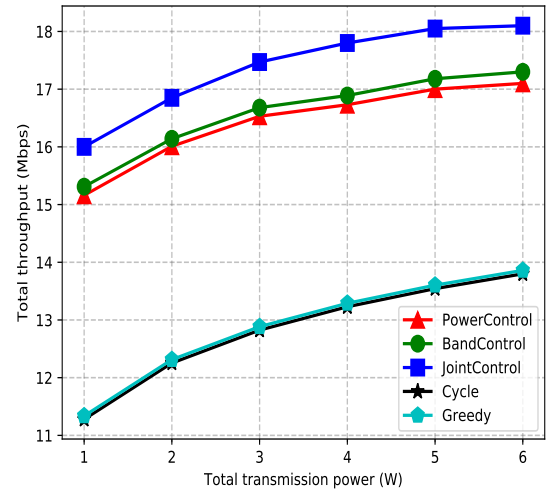
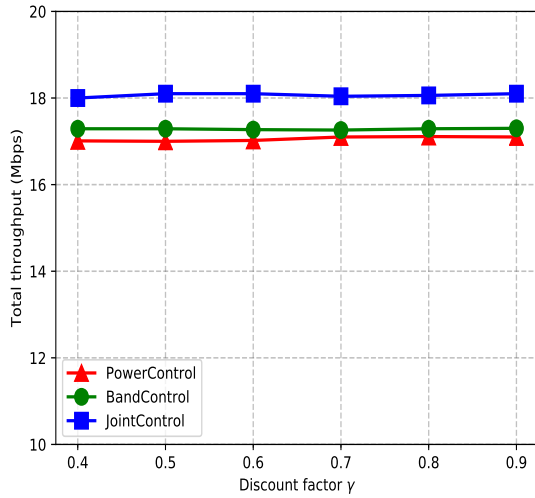


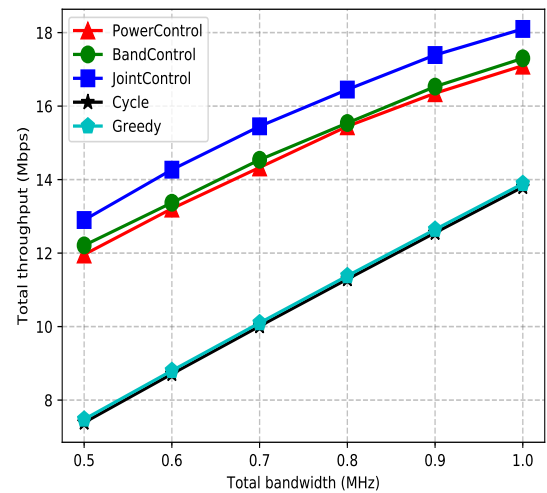
Fig. 8. Convergence of loss functions in training stage.

Fig. 10. Total throughput vs. total transmission power ($B = 1$ MHz).Fig. 9. Throughput vs. discount factor γ .

when γ changes, the throughput of three algorithms is steady; and JointControl achieves higher total throughput, comparing with PowerControl and BandControl, respectively.

Total throughput vs. total transmission power ($P = 1 \sim 6$) and total bandwidth ($B = 0.5 \sim 1$ MHz) are shown by Fig. 10 and Fig. 11, where we set $\lambda = 0.5$ and $\gamma = 0.9$. We see that DDPG achieves the best performance for different transmission power and bandwidth budgets, respectively. Moreover, the total throughput of all algorithms increases when the total transmission power or bandwidth increases. PowerControl and BandControl only adjust the transmission power or bandwidth, while JointControl jointly adjusts both of them, so its performance is the best. The total throughput of DDPG-based algorithms is improved greatly than that of Cycle and Greedy. The performance of Greedy is a little better than Cycle, since Greedy tries to get nearer to the block with the largest number of vehicles.

Total throughput vs. vehicle arrival probability λ is shown

Fig. 11. Total throughput vs. total bandwidth ($P = 6$ W).

in Fig. 12. Note that the road intersection has a capacity of 2 units, i.e., it can serve at most two traffic flows at the same time, therefore, it cannot serve traffic flows where λ is very high, e.g., $\lambda = 0.8$ and $\lambda = 0.9$. We see that, when λ increases, i.e., more vehicles arrive at the intersection, the total throughput increases. However, when λ gets higher, e.g., $\lambda = 0.6$, the total throughput saturates due to traffic congestion.

Next, we test the energy consumption of 3D flight in the proposed solutions. Our setups follow the UAV DJI MATRICE 100 [45]. We assume that the UAV has three vertical flight actions per time slot, i.e., moving downward 5 meters, horizontally, and upward 5 meters. If the UAV keeps moving downward, horizontally, or upward until the energy for 3D flight is used up, the flight time is assumed to be 30, 22, and 14 minutes, respectively. The duration of a time slot is set to

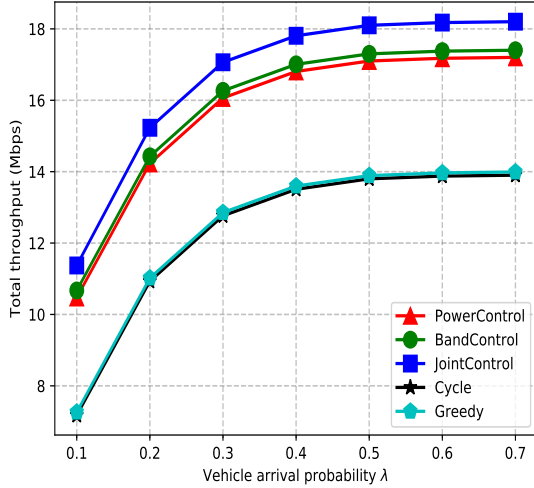
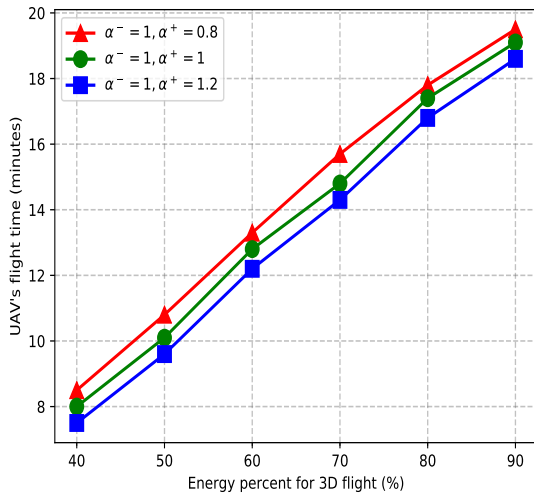
Fig. 12. Total throughput vs. vehicle arrival probability λ .

Fig. 13. UAV's flight time vs. energy percent for 3D flight in JointControl.

6 seconds, so the UAV can fly 300, 220, and 140 time slots, respectively. The experience replay buffer capacity is set to 50, and the mini-batch size M is set to 25.

The UAV's flight time vs. energy percent for 3D flight in JointControl is shown in Fig. 13. When $\alpha^- = 1, \alpha^+ = 1.2$, the UAV's flight time is shorter than that of the other cases, since the UAV is active. When $\alpha^- = 1, \alpha^+ = 0.8$, the UAV's flight time is the longest since the UAV is inactive. When $\alpha^- = \alpha^+ = 1$, the UAV's flight time is between the other two cases. If the energy percent for 3D flight increases, the UAV's flight time increases linearly in the three cases.

VI. DISCUSSION AND CONCLUSION

We studied a UAV-assisted vehicular network where the UAV acted as a relay to maximize the total throughput between the UAV and vehicles. We focused on the downlink

communication where the UAV could adjust its transmission power and bandwidth allocation under 3D flight. We formulated this problem as a MDP problem, explored the state transitions of UAV and vehicles under different actions, and then proposed three deep reinforcement learning schemes based on the DDPG algorithms, and finally extend them on energy consumption of the UAV's 3D flight. In a simplified scenario with small state space and action space, we verify the optimality of DDPG-based algorithms. Through simulation results, we demonstrated the performance of the algorithms under a more realistic traffic scenario, comparing with two baseline schemes.

In the future, we will consider the scenario where multiple UAVs constitute a relay network to assist vehicular networks and study the coverage overlap/probability, relay selection, energy-aware communications, and UAV cooperative communication protocols.

REFERENCES

- [1] M. Chaqfeh, H. El-Sayed, and A. Lakas, "Efficient data dissemination for urban vehicular environments," *IEEE Transactions on Intelligent Transportation Systems (TITS)*, no. 99, pp. 1–11, 2018.
- [2] M. Zhu, X.-Y. Liu, F. Tang, M. Qiu, R. Shen, W. Shu, and M.-Y. Wu, "Public vehicles for future urban transportation," *IEEE Transactions on Intelligent Transportation Systems (TITS)*, vol. 17, no. 12, pp. 3344–3353, 2016.
- [3] M. Zhu, X.-Y. Liu, and X. Wang, "Joint transportation and charging scheduling in public vehicle systems - a game theoretic approach," *IEEE Transactions on Intelligent Transportation Systems (TITS)*, vol. 19, no. 8, pp. 2407–2419, 2018.
- [4] M. Zhu, X.-Y. Liu, and X. Wang, "An online ride-sharing path-planning strategy for public vehicle systems," *IEEE Transactions on Intelligent Transportation Systems (TITS)*, vol. 20, no. 2, pp. 616–627, 2019.
- [5] M. Zhu, X.-Y. Liu, L. Kong, R. Shen, W. Shu, and M.-Y. Wu, "The charging-scheduling problem for electric vehicle networks," in *IEEE Wireless Communications and Networking Conference (WCNC)*, pp. 3178–3183, 2014.
- [6] M. Zhu, J. Hu, L. Kong, R. Shen, W. Shu, and M.-Y. Wu, "An algorithm of lane change using two-lane nasch model in traffic networks," in *IEEE International Conference on Connected Vehicles and Expo (ICCVE)*, pp. 241–246, 2013.
- [7] K. Li, C. Yuen, S. S. Kanhere, K. Hu, W. Zhang, F. Jiang, and X. Liu, "An experimental study for tracking crowd in smart cities," *IEEE Systems Journal*, 2018.
- [8] F. Cunha, L. Villas, A. Boukerche, G. Maia, A. Viana, R. A. Mini, and A. A. Loureiro, "Data communication in vanets: Protocols, applications and challenges," *Elsevier Ad Hoc Networks*, vol. 44, pp. 90–103, 2016.
- [9] H. Sedjelmaci, S. M. Senouci, and N. Ansari, "Intrusion detection and ejection framework against lethal attacks in uav-aided networks: a bayesian game-theoretic methodology," *IEEE Transactions on Intelligent Transportation Systems (TITS)*, vol. 18, no. 5, pp. 1143–1153, 2017.
- [10] "Paving the path to 5g: Optimizing commercial lte networks for drone communication (2018)," <https://www.qualcomm.cn/videos/paving-path-5g-optimizing-commercial-lte-networks-drone-communication>.
- [11] "Huawei signs mou with china mobile sichuan and fonair aviation to build cellular test networks for logistics drones (2018)," <https://www.huawei.com/en/press-events/news/2018/3/MoU-ChinaMobile-FonairAviation-Logistics>.
- [12] M. Alzenad, A. El-Keyi, F. Lagum, and H. Yanikomeroglu, "3-d placement of an unmanned aerial vehicle base station (uav-bs) for energy-efficient maximal coverage," *IEEE Wireless Communications Letters (WCL)*, vol. 6, no. 4, pp. 434–437, 2017.
- [13] M. Giordani, M. Mezzavilla, S. Rangan, and M. Zorzi, "An efficient uplink multi-connectivity scheme for 5g mmwave control plane applications," *IEEE Transactions on Wireless Communications (TWC)*, 2018.
- [14] Q. Yang and S.-J. Yoo, "Optimal uav path planning: Sensing data acquisition over iot sensor networks using multi-objective bio-inspired algorithms," *IEEE Access*, vol. 6, pp. 13671–13684, 2018.

[15] M. Garraffa, M. Bekhti, L. Létocart, N. Achir, and K. Boussetta, “Drones path planning for wsn data gathering: A column generation heuristic approach,” in *IEEE Wireless Communications and Networking Conference (WCNC)*, pp. 1–6, 2018.

[16] C. H. Liu, Z. Chen, J. Tang, J. Xu, and C. Piao, “Energy-efficient uav control for effective and fair communication coverage: A deep reinforcement learning approach,” *IEEE Journal on Selected Areas in Communications (JSAC)*, vol. 36, no. 9, pp. 2059–2070, 2018.

[17] H. Wang, G. Ding, F. Gao, J. Chen, J. Wang, and L. Wang, “Power control in uav-supported ultra dense networks: Communications, caching, and energy transfer,” *IEEE Communications Magazine*, vol. 56, no. 6, pp. 28–34, 2018.

[18] S. Yan, M. Peng, and X. Cao, “A game theory approach for joint access selection and resource allocation in uav assisted iot communication networks,” *IEEE Internet of Things Journal (IOTJ)*, 2018.

[19] Y. Wu, J. Xu, L. Qiu, and R. Zhang, “Capacity of uav-enabled multicast channel: Joint trajectory design and power allocation,” in *IEEE International Conference on Communications (ICC)*, pp. 1–7, 2018.

[20] Y. Zeng, X. Xu, and R. Zhang, “Trajectory design for completion time minimization in uav-enabled multicasting,” *IEEE Transactions on Wireless Communications (TWC)*, vol. 17, no. 4, pp. 2233–2246, 2018.

[21] S. Zhang, Y. Zeng, and R. Zhang, “Cellular-enabled uav communication: Trajectory optimization under connectivity constraint,” in *IEEE International Conference on Communications (ICC)*, pp. 1–6, 2018.

[22] R. Fan, J. Cui, S. Jin, K. Yang, and J. An, “Optimal node placement and resource allocation for uav relaying network,” *IEEE Communications Letters*, vol. 22, no. 4, pp. 808–811, 2018.

[23] U. Challita, W. Saad, and C. Bettstetter, “Deep reinforcement learning for interference-aware path planning of cellular-connected uavs,” in *IEEE International Conference on Communications (ICC)*, 2018.

[24] X.-Y. Liu, Z. Ding, S. Borst, and A. Walid, “Deep reinforcement learning for intelligent transportation systems,” in *NeurIPS Workshop on Machine Learning for Intelligent Transportation Systems*, 2018.

[25] A. Al-Hourani, S. Kandeepan, and S. Lardner, “Optimal lap altitude for maximum coverage,” *IEEE Wireless Communications Letters (WCL)*, vol. 3, no. 6, pp. 569–572, 2014.

[26] M. Mozaffari, W. Saad, M. Bennis, and M. Debbah, “Unmanned aerial vehicle with underlaid device-to-device communications: Performance and tradeoffs,” *IEEE Transactions on Wireless Communications (TWC)*, vol. 15, no. 6, pp. 3949–3963, 2016.

[27] D. Oehmann, A. Awada, I. Viering, M. Simsek, and G. P. Fettweis, “SINR model with best server association for high availability studies of wireless networks,” *IEEE Wireless Communications Letters (WCL)*, vol. 5, no. 1, pp. 60–63, 2015.

[28] V. Vahidi, E. Saberian, and B. T. Morris, “Ofdm performance assessment for traffic surveillance in drone small cells,” *IEEE Transactions on Intelligent Transportation Systems (TITS)*, 2018.

[29] P. Ramezani and A. Jamalipour, “Throughput maximization in dual-hop wireless powered communication networks,” *IEEE Transactions on Vehicular Technology (TVT)*, vol. 66, no. 10, pp. 9304–9312, 2017.

[30] C. J. Watkins and P. Dayan, “Q-learning,” *Springer Machine learning*, vol. 8, no. 3-4, pp. 279–292, 1992.

[31] C. Wirth and G. Neumann, “Model-free preference-based reinforcement learning,” in *AAAI Conference on Artificial Intelligence*, 2016.

[32] R. S. Sutton and A. G. Barto, *Reinforcement learning: An introduction*. MIT press, 2018.

[33] H. Van Hasselt, A. Guez, and D. Silver, “Deep reinforcement learning with double q-learning,” in *AAAI Conference on Artificial Intelligence*, 2016.

[34] T. P. Lillicrap, J. J. Hunt, A. Pritzel, N. Heess, T. Erez, Y. Tassa, D. Silver, and D. Wierstra, “Continuous control with deep reinforcement learning,” in *International Conference on Learning Representations (ICLR)*, 2016.

[35] D. Silver, J. Schrittwieser, K. Simonyan, I. Antonoglou, A. Huang, A. Guez, T. Hubert, L. Baker, M. Lai, A. Bolton, et al., “Mastering the game of go without human knowledge,” *Nature*, vol. 550, no. 7676, p. 354, 2017.

[36] V. Mnih, K. Kavukcuoglu, D. Silver, A. Graves, I. Antonoglou, D. Wierstra, and M. Riedmiller, “Playing atari with deep reinforcement learning,” *arXiv preprint arXiv:1312.5602*, 2013.

[37] P.-W. Chou, D. Maturana, and S. Scherer, “Improving stochastic policy gradients in continuous control with deep reinforcement learning using the beta distribution,” in *International Conference on Machine Learning (ICML)*, pp. 834–843, 2017.

[38] A. Daniely, “Sgd learns the conjugate kernel class of the network,” in *Advances in Neural Information Processing Systems (NIPS)*, pp. 2422–2430, 2017.

[39] V. Nair and G. E. Hinton, “Rectified linear units improve restricted boltzmann machines,” in *International conference on machine learning (ICML)*, pp. 807–814, 2010.

[40] K. He, X. Zhang, S. Ren, and J. Sun, “Delving deep into rectifiers: Surpassing human-level performance on imagenet classification,” in *IEEE international conference on computer vision (ICCV)*, pp. 1026–1034, 2015.

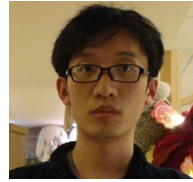
[41] G. Lefebvre, M. Lebreton, F. Meyniel, S. Bourgeois-Gironde, and S. Palminteri, “Behavioural and neural characterization of optimistic reinforcement learning,” *Nature Human Behaviour*, vol. 1, no. 4, p. 0067, 2017.

[42] M. Abadi, P. Barham, J. Chen, Z. Chen, A. Davis, J. Dean, M. Devin, S. Ghemawat, G. Irving, M. Isard, et al., “Tensorflow: A system for large-scale machine learning,” in *USENIX Symposium on Operating Systems Design and Implementation (OSDI)*, pp. 265–283, 2016.

[43] “Python markov decision process (mdp) toolbox (2019).” <https://pymdptoolbox.readthedocs.io/en/latest/api/mdptoolbox.html>.

[44] M. Mozaffari, W. Saad, M. Bennis, and M. Debbah, “Drone small cells in the clouds: Design, deployment and performance analysis,” in *IEEE Global Communications Conference (GLOBECOM)*, pp. 1–6, 2015.

[45] “Homepage of dji matrice 100 (2019).” <https://www.dji.com/cn/matrice100/info>.



Ming Zhu received the Ph.D. degree in Computer Science and Engineering in Shanghai Jiao Tong University, Shanghai, China. He is now a Post-Doctoral Researcher and an Assistant Researcher in Shenzhen Institutes of Advanced Technology, Chinese Academy of Sciences, Shenzhen, China.

His research interests are in the area of big data, artificial intelligence, intelligent transportation systems, smart cities, and wireless communications.



Xiao-Yang Liu received the B.Eng. degree in Computer Science from Huazhong University of Science and Technology, and the PhD degree in the Department of Computer Science and Engineering, Shanghai Jiao Tong University, China. He is currently a PhD in the Department of Electrical Engineering, Columbia University.

His research interests include tensor theory, deep learning, non-convex optimization, big data analysis and IoT applications.



Xiaodong Wang (S'98-M'98-SM'04-F'08) received the Ph.D. degree in electrical engineering from Princeton University. He is currently a Professor of electrical engineering with Columbia University, New York NY, USA. His research interests fall in the general areas of computing, signal processing, and communications. He has authored extensively in these areas. He has authored the book entitled *Wireless Communication Systems: Advanced Techniques for Signal Reception*, (Prentice Hall, 2003).

His current research interests include wireless communications, statistical signal processing, and genomic signal processing. He has served as an Associate Editor of the *IEEE TRANSACTIONS ON COMMUNICATIONS*, *IEEE TRANSACTIONS ON WIRELESS COMMUNICATIONS*, *IEEE TRANSACTIONS ON SIGNAL PROCESSING*, and *IEEE TRANSACTIONS ON INFORMATION THEORY*. He is an ISI Highly Cited Author. He received the 1999 NSF CAREER Award, the 2001 IEEE Communications Society and Information Theory Society Joint Paper Award, and the 2011 IEEE Communication Society Award for Outstanding Paper on New Communication Topics.